

Shape of ^{44}Ar: Onset of deformation in neutron rich nuclei near ^{48}Ca

M. Zielinska, A. Görgen, E. Clément, J. P. Delaroche, M. Girod, W. Korten, A. Burger, W. Catford, C. Dossat, J. Iwanicki, et al.

▶ **To cite this version:**

M. Zielinska, A. Görgen, E. Clément, J. P. Delaroche, M. Girod, et al.. Shape of ^{44}Ar: Onset of deformation in neutron rich nuclei near ^{48}Ca. Physical Review C, 2009, 80, pp.014317. 10.1103/PhysRevC.80.014317 . in2p3-00403065

HAL Id: in2p3-00403065
https://hal.in2p3.fr/in2p3-00403065

Submitted on 15 Jul 2009

HAL is a multi-disciplinary open access archive for the deposit and dissemination of scientific research documents, whether they are published or not. The documents may come from teaching and research institutions in France or abroad, or from public or private research centers.

L'archive ouverte pluridisciplinaire **HAL**, est destinée au dépôt et à la diffusion de documents scientifiques de niveau recherche, publiés ou non, émanant des établissements d'enseignement et de recherche français ou étrangers, des laboratoires publics ou privés.

On the shape of ^{44}Ar: Onset of deformation in neutron-rich nuclei near ^{48}Ca

M. Zielińska,[1,2] A. Görgen,[1] E. Clément,[1,*] J.-P. Delaroche,[3] M. Girod,[3]
W. Korten,[1] A. Bürger,[1,4,†] W. Catford,[5] C. Dossat,[1] J. Iwanicki,[2]
J. Libert,[6] J. Ljungvall,[1,*] P.J. Napiorkowski,[2] A. Obertelli,[1] D. Piętak,[7]
R. Rodríguez-Guzmán,[8] G. Sletten,[9] J. Srebrny,[2] Ch. Theisen,[1] and K. Wrzosek[2]

[1]*CEA Saclay, IRFU, Service de Physique Nucléaire, F-91191 Gif-sur-Yvette, France*
[2]*Heavy Ion Laboratory, University of Warsaw, PL-02-093 Warsaw, Poland*
[3]*CEA, DAM, DIF, F-91297 Arpajon, France*
[4]*Helmholtz Institut für Strahlen- und Kernphysik,*
Universität Bonn, D-53115 Bonn, Germany
[5]*Department of Physics, University of Surrey,*
Guildford, GU2 7XH, United Kingdom
[6]*Institut de Physique Nucléaire, IN2P3-CNRS/Université Paris-Sud, F-91406 Orsay, France*
[7]*II WeiTI, Warsaw University of Technology, Poland*
[8]*Department of Physics, University of Jyväskylä,*
P.O. Box 35, FI-40014 Jyväskylä, Finland
[9]*Niels Bohr Institute, University of Copenhagen, DK-2100 Copenhagen, Denmark*

(Dated: June 2, 2009)

Abstract

The development of deformation and shape coexistence in the vicinity of doubly-magic ^{48}Ca, related to the weakening of the $N = 28$ shell closure, was addressed in a low-energy Coulomb excitation experiment using a radioactive ^{44}Ar beam from the SPIRAL facility at GANIL. The 2_1^+ and 2_2^+ states in ^{44}Ar were excited on ^{208}Pb and ^{109}Ag targets at two different beam energies. $B(E2)$ values between all observed states and the spectroscopic quadrupole moment of the 2_1^+ state were extracted from the differential Coulomb excitation cross sections, indicating prolate shape of the ^{44}Ar nucleus, and giving evidence for an onset of deformation already two protons and two neutrons away from doubly-magic ^{48}Ca. New Hartree-Fock-Bogoliubov based configuration mixing calculations have been performed with the Gogny D1S interaction for ^{44}Ar and neighboring nuclei using two different approaches: the angular-momentum projected generator coordinate method considering axial quadrupole deformations and a five-dimensional approach including the triaxial degree of freedom. The experimental values and new calculations are furthermore compared to the shell model and to relativistic mean field calculations. The new results give insight into the weakening of the $N = 28$ shell closure and the development of deformation in this neutron-rich region of the nuclear chart.

PACS numbers: 21.60.-n, 23.20.Js, 25.70.De, 27.40.+z

*Present address: GANIL, BP-5027, F-14076 Caen, France

†Present address: SAFE, University of Oslo, N-0316 Oslo, Norway

I. INTRODUCTION

The shape of the atomic nucleus reflects very sensitively the underlying shell structure of the nucleons. Nuclei in the vicinity of closed shells are generally spherical. The presence of only few valence particles (or holes) is usually not sufficient to polarize the stiff 'magic' core and induce deformation. Away from closed shells, on the other hand, the valence nucleons can scatter into various orbitals near the Fermi surface. Since the energies of the orbitals change with deformation, in particular for intruder orbitals from the next major shell, the nucleus can minimize its energy by assuming a deformed shape.

Following this argumentation, nuclei in the vicinity of doubly-magic ^{48}Ca should be spherical. However, it is known that the shell structure changes when moving away from the valley of stability: The large energy gaps at the magic numbers present in stable nuclei can get washed out, and new shell gaps at other nucleon numbers may appear. The fundamental question of how the nuclear shell structure evolves with proton or neutron excess is one of the main motivations to study nuclei far from stability. The study of the shape of such exotic nuclei can reveal changes in the shell structure and is a particularly sensitive test of nuclear structure models and their predictive power.

The disappearance of a shell closure in neutron-rich nuclei was first discovered in the so-called 'island of inversion' at $N = 20$, where the ground states of neutron-rich Na, Mg and Ne isotopes are dominated by deformed intruder configurations [1]. While the $N = 20$ shell closure disappears rather abruptly between ^{34}Si and ^{32}Mg, evidence has been accumulated recently for a more gradual erosion of the neutron shell closure in the proton-deficient $N = 28$ isotones below ^{48}Ca. The shell closure at $N = 28$ is the first one driven by the spin-orbit interaction and, unlike $N = 20$, separates orbitals of the same parity. Neutron single-particle energies have been determined via the $d(^{46}\mathrm{Ar},^{47}\mathrm{Ar})p$ reaction, indicating a moderate reduction of the $N = 28$ gap for ^{46}Ar [2]. A rather low-lying and collective 2^+_1 state in ^{44}S [3] and the presence of an isomeric 0^+_2 state at low excitation energy [4] suggest the presence of deformation and shape coexistence in ^{44}S. The g-factor measurement of a low-lying isomeric state in ^{43}S established a $\nu f_{7/2}$ configuration of this state and an intruder character of the ground state [5]. Finally, the very low-lying 2^+_1 state at only 770 keV in ^{42}Si [6] provides evidence for a substantial deformation and the complete collapse of the $N = 28$ shell closure at $Z = 14$. This result is at variance with an earlier interpretation based on the measurement

of the two proton knock-out cross section, which concluded that a strong $Z = 14$ subshell closure will result in a spherical 'magic' nucleus [7].

Large-scale shell model calculations with the full proton *sd* and neutron *pf* shells as valence space originally predicted the persistence of the $N = 28$ shell closure and a doubly-magic character of ^{42}Si [8]. As more experimental data became available, the effective interaction was adjusted, and shell model calculations are now reproducing the experimentally observed collapse of the shell closure [9]. The erosion of the shell closure and the development of deformation for the proton-deficient $N = 28$ isotones was also predicted by Skyrme Hartree-Fock and relativistic mean-field (RMF) calculations [10, 11]. Fully self-consistent relativistic Hartree-Bogoliubov calculations predicted a staggering of the ground-state deformation between oblate in ^{46}Ar and ^{42}Si and prolate in ^{44}S and ^{40}Mg, while the absolute deformation was found to increase with decreasing proton number [12]. Spectroscopic properties of $N = 28$ isotones were calculated using the angular momentum projected generator coordinate method with the axial quadrupole moment as generator coordinate and the Gogny D1S interaction [13]. These calculations predicted the onset of deformation for ^{46}Ar and coexistence of well-deformed oblate and prolate shapes in the lighter isotones, with oblate shapes favored in ^{44}S and ^{42}Si, and prolate deformation dominating in ^{40}Mg.

The nuclear shape changes not only rapidly with the proton but also with the neutron number in this region of the nuclear chart. Spectroscopic results in the neutron-rich sulfur isotopes, for example, are consistent with a transition from prolate deformation in ^{40}S via γ-softness in ^{42}S to prolate-oblate shape coexistence in ^{44}S [14]. This interpretation is supported by Hartree-Fock-Bogoliubov based configuration mixing calculations using a five-dimensional collective Hamiltonian and the Gogny D1S interaction [14, 15]. These calculations predict that oblate shapes become favored in the $N = 30$ isotope ^{46}S.

The spectroscopy of proton-deficient nuclei with $N \approx 28$ is very challenging and at the very limits of feasibility with present-day techniques. $B(E2)$ values have been measured via intermediate-energy Coulomb excitation for ^{44}Ar [16], ^{46}Ar [16, 17], $^{38-42}$S [16], and ^{44}S [3]. Only the excitation energy of the 2_1^+ state is known in ^{42}Si [6], while a measurement of the $B(E2)$ value for this nucleus is presently out of reach. The drip-line nucleus ^{40}Mg, finally, was recently observed for the first time by identifying three events in a fragmentation experiment [18]. The measurement of the energy and excitation probability of the first excited state gives a first indication of the collectivity of a nucleus. The measurement of quadrupole moments

and the excitation probability of non-yrast states provides more profound nuclear-structure information. Such measurements require radioactive ion beams of high quality and intensity at energies well below the Coulomb barrier and have so far never been attempted in this region of the nuclear chart. In this work we report on the measurement of the spectroscopic quadrupole moment and the $B(E2)$ values to the 2_1^+ and 2_2^+ states in ^{44}Ar. The precise measurement of these observables via low-energy Coulomb excitation and the reorientation effect gives insight into the development of deformation in this region of the nuclear chart and serves as a stringent test for both microscopic collective and shell models.

Spectroscopic data on ^{44}Ar had been obtained previously using various techniques to populate excited states. The resulting level schemes above the 2_1^+ state at 1158 keV, however, are inconsistent. A sequence comprising a 2^+, 4^+, and 6^+ state at 1158, 2746, and 3439 keV was proposed based on the γ rays observed following deep-inelastic reactions [19]. On the other hand, a direct transition from a state at 2748 keV to the ground state was observed following the β decay of ^{44}Cl [20], casting doubt on the (tentative) assignment of spin-parity 4^+ for the state observed after deep-inelastic collisions. A second 2^+ state was reported at an excitation energy of 1.78 MeV in an experiment using nucleon removal reactions at relativistic energies [21]. Other experiments do not confirm the presence of a 2^+ state at this energy. The 2_2^+ state was reported at an excitation energy of 2011 keV in the β-decay study [20]. Finally, the $B(E2; 0_1^+ \rightarrow 2_1^+)$ value for ^{44}Ar has been measured using Coulomb excitation at intermediate energy [16], and the density distribution has been probed using inelastic proton scattering [22].

Low-energy Coulomb excitation can provide valuable complementary information to the existing data for the low-lying states in ^{44}Ar. The technique is in particular sensitive to diagonal matrix elements via second-order effects, which allow extracting quadrupole moments including their sign. In this way the deformation and shape associated with a given state can be measured. Low-energy Coulomb excitation is the only experimental technique which can distinguish between prolate and oblate shape of the nucleus in a short-lived excited state. Contrary to intermediate-energy Coulomb excitation, it is furthermore possible to excite higher lying states in multiple steps. The measurement of the differential excitation cross section for each state as a function of scattering angle yields a complete set of matrix elements connecting all states populated in the experiment. Also the spin-parity of the excited states can usually be inferred from the observed excitation probabilities. In this work

we report on the results of a projectile Coulomb excitation experiment with radioactive ^{44}Ar beam at 'safe' energy below the Coulomb barrier.

The paper is organized as follows: Experimental details are presented in Sec. II, followed by a description of the data analysis procedure and the presentation of the results in Sec. III. The results are discussed and compared with shell model, mean-field, and beyond-mean-field calculations in Sec. IV. Finally, the work is summarized and conclusions are drawn in Sec. V.

II. EXPERIMENTAL DETAILS

A radioactive ^{44}Ar beam was produced at the SPIRAL facility [24] at GANIL using the Isotope Separation On-Line (ISOL) technique. An intense ^{48}Ca primary beam was accelerated subsequently by the two large sector-separated cyclotrons of GANIL to an energy of $60A$ MeV with an average beam current of 3.5 $e\mu$A. The ^{48}Ca projectiles were fragmented on the carbon production target of SPIRAL, which was operated at high temperature to facilitate the migration of the radioactive atoms to the surface. From there the reaction products diffused into a Nanogan-3 [25] ECR ion source via a cold transfer tube, which largely prevented non-gaseous elements from reaching the plasma of the source. Radioactive ^{44}Ar atoms ($T_{1/2} = 11.9$ min) were ionized to charge state 8+ and transported to the CIME cyclotron for re-acceleration. The cyclotron itself provides at the same time a high mass resolution resulting in a quasi-pure secondary beam.

In order to exploit the strong Z dependence of the Coulomb excitation cross section, the experiment was split into two parts during which the re-accelerated ^{44}Ar projectiles were impinging on ^{109}Ag and ^{208}Pb secondary targets at energies of $2.68A$ and $3.68A$ MeV, respectively. The secondary beam energies were chosen such that the distance of closest approach d fulfilled the condition

$$d \geq 1.25(A_p^{1/3} + A_t^{1/3}) + 5 \text{ fm}, \tag{1}$$

which ensures a purely electromagnetic excitation [26]. While Coulomb excitation of the doubly-magic nucleus ^{208}Pb is negligible under these conditions, the ^{109}Ag target nuclei are easily excited, which can be used for normalization purposes. The ^{109}Ag and ^{208}Pb targets had thicknesses of 1.0 and 0.9 mg/cm^2, respectively. The average intensity of the secondary beam was 2×10^5 ions per second at the target position.

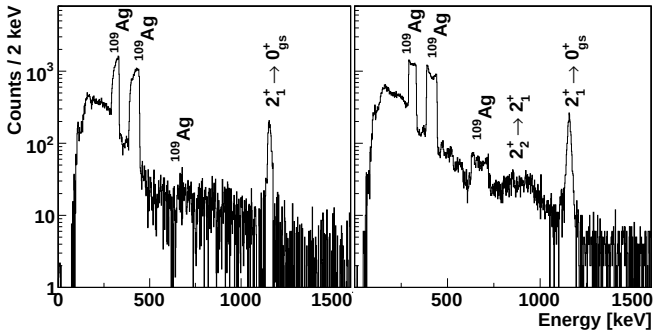


FIG. 1: Total γ-ray spectra after Coulomb excitation of ^{44}Ar on a ^{109}Ag target in coincidence with ^{44}Ar ejectiles (left) and ^{109}Ag recoils (right), corresponding to small and large center-of-mass scattering angles, respectively. The spectra are Doppler corrected using the velocity vector of the ^{44}Ar projectiles.

The γ rays from the Coulomb excited states were detected in the EXOGAM array [27], which comprised 10 large escape-suppressed germanium clover detectors for this experiment. Each clover detector consists of four HPGe crystals, the outer contacts of which are electrically segmented into four segments, giving precise spacial information on the energy deposit in the detectors. The scattered projectiles and the recoiling target nuclei were detected in an annular double-sided silicon detector, divided into 16 concentric rings on the front and 96 azimuthal sectors on the back side. The active surface of the detector had inner and outer radii of 9 and 41 mm, respectively, and it was placed 25 mm downstream from the target. The energy resolution of the particle detector was sufficient to distinguish between scattered projectiles and target recoils, thereby allowing the kinematic reconstruction of the Coulomb excitation events. The segmentation of both the silicon and the germanium detectors resulted in a precise measurement of the emission angle of the γ rays with respect to the velocity vector of the scattered projectile. A resolution of 10 keV was obtained for a γ ray of 1158 keV after Doppler correction. The coincidence requirement between γ rays detected in EXOGAM and scattered particles detected in the silicon detector helped to suppress the otherwise overwhelming background from the β decay of the beam.

Both projectile and target nuclei can be excited in a collision between ^{44}Ar and ^{109}Ag. The well-known transition strengths in ^{109}Ag [28, 29] can thus be used to normalize the excitation probability in ^{44}Ar. The Doppler-corrected γ-ray spectra in coincidence with scattered ^{44}Ar ions and ^{109}Ag recoils are shown in Fig.1. Projectile and target detection correspond to small

and large scattering angles in the center-of-mass system, respectively. The dependence of the excitation process on the scattering angle is clearly visible, for example the enhancement for large scattering angles of the $9/2^- \rightarrow 5/2^-$ transition at 676 keV in ^{109}Ag, which requires a multi-step excitation.

The statistics collected during ∼50 hours of data taking with the ^{109}Ag target allowed subdividing the data into four sub-sets corresponding to different ranges of scattering angles as shown in Table I. The ranges A and B correspond to the detection of scattered ^{44}Ar projectiles, while the ranges C and D correspond to detection of the recoiling target nuclei. The overlap between the different ranges are due to a misalignment of the beam with respect to the particle detector. This displacement was estimated to be 2.8(2) mm from the energy of scattered beam particles measured by individual azimuthal sectors for each of the rings. This misalignment was taken into account in the Doppler correction procedure and the Coulomb excitation analysis.

The influence of the quadrupole moment of the 2_1^+ state in ^{44}Ar on its excitation probability varies significantly with the scattering angle. It is hence possible to extract both the transitional and diagonal matrix elements involved in the excitation process from a differential measurement of the excitation cross section. The division of the data into angular ranges was a compromise between the number of independent data points for the γ-ray yields and the minimum level of statistics obtained for the individual ranges. It was chosen to use wider ranges for large scattering angles, where the influence of the quadrupole moment on the population of the 2_1^+ state is strongest, in order to determine the corresponding γ-ray yields with higher accuracy.

In the second part of the experiment data was collected for ∼100 hours with a ^{208}Pb target at a beam energy of $3.68A$ MeV. The higher Z of the target material results in larger cross sections, so that higher-lying states in ^{44}Ar became accessible. In addition to the 2_1^+ state, the level at 2011 keV, which was already observed after β decay of ^{44}Cl and tentatively assigned as 2_2^+ [20], was populated and its de-excitation via two γ rays to the 2_1^+ and the ground state was observed. The $2_2^+ \rightarrow 2_1^+$ transition is partly overlapping with the Compton edge of the $2_1^+ \rightarrow 0_1^+$ transition, hampering the precise determination of its intensity. The decay scheme of the states which were populated by Coulomb excitation on the ^{208}Pb target is shown in Fig. 2 together with the Doppler-corrected, background subtracted γ-ray spectrum in coincidence with ^{208}Pb recoils. The resulting γ-ray yields are

TABLE I: Measured γ-ray yields (without efficiency correction) for scattering on ^{109}Ag and ^{208}Pb targets, respectively. The ranges of scattering angles are given in the center of mass frame.

Data set	Nucleus	Transition	Counts	Error
A	^{44}Ar	$2_1^+ \rightarrow 0_1^+$	493	34
[22.1°,50.0°]	^{109}Ag	$3/2_1^- \rightarrow 1/2_1^-$	6280	110
		$5/2_1^- \rightarrow 1/2_1^-$	6690	110
B	^{44}Ar	$2_1^+ \rightarrow 0_1^+$	1154	58
[37.9°,78.6°]	^{109}Ag	$3/2_1^- \rightarrow 1/2_1^-$	13100	250
		$5/2_1^- \rightarrow 1/2_1^-$	13740	220
C	^{44}Ar	$2_1^+ \rightarrow 0_1^+$	1575	58
[61.8°,105.0°]		$2_2^+ \rightarrow 2_1^+$	48	20
	^{109}Ag	$3/2_1^- \rightarrow 1/2_1^-$	12430	230
		$5/2_1^- \rightarrow 1/2_1^-$	13240	200
D	^{44}Ar	$2_1^+ \rightarrow 0_1^+$	1274	54
[92.1°,148.3°]		$2_2^+ \rightarrow 2_1^+$	54	26
	^{109}Ag	$3/2_1^- \rightarrow 1/2_1^-$	11050	220
		$5/2_1^- \rightarrow 1/2_1^-$	11530	210
E	^{44}Ar	$2_1^+ \rightarrow 0_1^+$	2243	73
[62.8°,153.4°]		$2_2^+ \rightarrow 2_1^+$	113	24
		$2_2^+ \rightarrow 0_1^+$	39	11
	^{208}Pb	–	–	–

given in Table I (range E).

During this part of the experiment a beam halo of poorly focused ^{44}Ar ions of different charge state was present due to charge-exchange reactions with the residual gas in the beam line. Direct hits of these particles on the inner part of the silicon detector (of the order of 1000/s) could not be cleanly distinguished from scattered beam particles and lead to an increased background of random coincidences with the decay of the highly radioactive beam. In order to exclude systematic errors originating from this background, small scattering angles were not considered in the analysis of the data taken with the ^{208}Pb target.

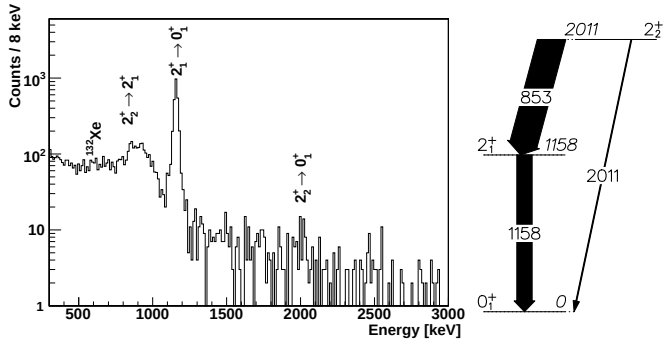


FIG. 2: Total Doppler-corrected γ-ray spectrum after Coulomb excitation of ^{44}Ar on a ^{208}Pb target in coincidence with ^{208}Pb recoils. The decay scheme of the populated states is shown on the right. The transitions are labeled with their energies (in keV), and the width of the arrows is proportional to the deduced $B(E2)$ values.

III. COULOMB EXCITATION ANALYSIS AND RESULTS

The Coulomb excitation least squares fitting code GOSIA [30] was used to determine transitional and diagonal $E2$ matrix elements. A χ^2 function is constructed from the observed γ-ray yields and those calculated from a set of matrix elements between all relevant states. The excitation probabilities are calculated in a semi-classical way [31] from a given set of matrix elements by integrating over the different ranges of scattering angles and the range of incident projectile energies resulting from their energy loss in the target foil. To calculate the γ-ray yields from the excitation probabilities, the geometry and relative efficiency of the detectors are taken into account. The γ-ray intensities are corrected for internal conversion, and the angular correlation of the γ rays is corrected for relativistic effects and the attenuation caused by the de-orientation effect during recoil into vacuum. The latter is caused by the interaction of the recoiling nucleus with the fluctuating hyperfine fields of the atomic electrons, which is treated in a simplifying phenomenological model [32, 33].

In a first step the influence of the quadrupole moment of the 2_1^+ state on its excitation probability was investigated at small scattering angles. For this purpose a GOSIA calculation was performed with the input data from the ^{109}Ag target restricted to the angular range A (see Table I) and with the $B(E2)$ fixed to the experimental value from intermediate-energy Coulomb excitation, $B(E2; 0_1^+ \rightarrow 2_1^+) = 345(41)\ e^2\text{fm}^4$ [16]. Changing the value of the quadrupole moment had only a negligible effect on the excitation probability compared

to the statistical uncertainty of the γ-ray yield. In an analog way it could be shown that higher-lying states have no significant influence on the excitation probability of the 2_1^+ state at the small scattering angles of range A. The γ-ray yield of set A for the 2_1^+ state depends therefore only on the transitional matrix element $\langle 0_1^+||\mathcal{M}(E2)||2_1^+\rangle$, which can consequently be obtained from data set A alone by normalizing to the excitation probability of states in the ^{109}Ag target nucleus. The uncertainty of the resulting $B(E2)$ value is dominated by the statistical error of the measured yields and the uncertainties of the matrix elements for the target nucleus ^{109}Ag [28].

In a second step, the remaining data sets (B-E) from both the ^{109}Ag and ^{208}Pb targets were analyzed simultaneously with the GOSIA code using the standard procedure of χ^2 minimization. The $B(E2; 0_1^+ \rightarrow 2_1^+)$ value determined from data set A and the branching ratio $I_\gamma(2_2^+ \rightarrow 0_1^+)/I_\gamma(2_2^+ \rightarrow 2_1^+)$ known from β-decay studies [20, 34] together with their experimental uncertainties were included as additional data points in the fit. The γ-ray yields measured for ^{109}Ag were used to determine the normalization factors related to the Rutherford cross-section and the efficiency of the particle detection for the subsets of data collected on the ^{109}Ag target. These normalization factors were then used when fitting matrix elements in ^{44}Ar to the observed γ-ray yields. To use the $B(E2)$ value which was derived independently from data set A as additional input data enhanced the sensitivity of the remaining data to the diagonal matrix element $\langle 2_1^+||\mathcal{M}(E2)||2_1^+\rangle$ and those related to the 2_2^+ state. The two-step analysis was found to reduce the uncertainties of the matrix elements compared to a one-step analysis, where the data from all angular ranges were fitted simultaneously. The resulting transitional and diagonal $E2$ matrix elements and the deduced $B(E2)$ values and the spectroscopic quadrupole moment are presented in Table II.

The reduced transition probability, $B(E2; 0_1^+ \rightarrow 2_1^+) = 378^{+34}_{-55}$ e^2fm^4, is in agreement with the value of 345(41) e^2fm^4 which was found in intermediate-energy Coulomb excitation [16]. Alternative subdivisions of the data into two, five, six, and eight angular ranges were tested and analyzed with GOSIA. The resulting sets of matrix elements were consistent, but the adopted division into four ranges was found to be the best compromise between the number of data points and the level of statistics for each data set, resulting in the highest accuracy for the quadrupole moment $Q_s(2_1^+)$. The measured value of $Q_s(2_1^+) = -8(3)$ $e$fm^2 represents experimental proof for prolate shape of the ^{44}Ar nucleus in the 2_1^+ state.

In the rotational model the spectroscopic quadrupole moment Q_s and the $B(E2)$ value

TABLE II: Reduced $E2$ matrix elements in ^{44}Ar obtained in the present work and resulting $B(E2)$ values and spectroscopic quadrupole moment.

I_1	I_2	$\langle I_2 \| E2 \| I_1 \rangle$ (eb)	$B(E2; I_1 \to I_2)$ (e^2fm^4)	Q_s ($e$fm^2)
0_1^+	2_1^+	$0.194^{+0.009}_{-0.015}$	378^{+34}_{-55}	
0_1^+	2_2^+	$0.048^{+0.004}_{-0.004}$	23^{+2}_{-2}	
2_1^+	2_2^+	$0.58^{+0.06}_{-0.04}$	680^{+150}_{-90}	
2_1^+	2_1^+	$-0.11^{+0.04}_{-0.04}$		$-8.3^{+3.0}_{-3.0}$

are related to the intrinsic quadrupole moment Q_0 as:

$$Q_s = Q_0 \frac{3K^2 - I(I+1)}{(I+1)(2I+3)}, \tag{2}$$

$$B(E2; I_1 \to I_2) = \frac{5}{16\pi} Q_0^2 \left| \langle I_1 K 20 | I_2 K \rangle \right|^2 . \tag{3}$$

For a purely vibrational nucleus, on the other hand, it is $Q_s = 0$. The intrinsic quadrupole moment obtained from the $B(E2; 0_1^+ \to 2_1^+)$ value in the rotational model is $Q_0 = +62^{+3}_{-4}$ $e$fm^2, which corresponds to $Q_s = -17.6^{+0.8}_{-1.3}$ $e$fm^2 and a quadrupole deformation of $\beta_2 = +0.23$. The measured spectroscopic quadrupole moment of $Q_s = -8(3)$ $e$fm^2 lies hence in between a rotational and a vibrational value. This argumentation, however, is only valid for a nucleus with axial symmetry. A potential triaxial deformation, which is difficult to prove experimentally, would also result in a lower spectroscopic quadrupole moment compared to axial symmetric deformation.

The spectroscopic quadrupole moment is also smaller than one would expect from the deformation parameter $|\beta_2| = 0.31(5)$ which was extracted from the inelastic proton scattering experiment [22]. While Coulomb excitation probes only the proton distribution, inelastic proton scattering at intermediate energy is also sensitive to the neutron distribution. The difference between the two results could therefore be explained by a stronger neutron deformation. One should keep in mind, however, that the extraction of a deformation parameter from inelastic proton scattering is model dependent. While the absolute magnitude of deformation extracted from inelastic proton scattering should be taken with care, a consistent picture emerges when comparing the relevant quantities with those of ^{36}Ar. The shape

of ^{36}Ar was found to be oblate with $Q_s(2_1^+) = +11(6)$ $e$fm^2 [35]. The proton scattering experiment, which is not sensitive to the sign of the deformation, found an absolute deformation parameter of $|\beta_2| = 0.36(4)$ for ^{36}Ar [22], slightly larger than for ^{44}Ar and consistent with the larger quadrupole moment. The smaller $B(E2)$ value of 300(30) e^2fm^4 and larger spectroscopic quadrupole moment suggests that ^{36}Ar has a more rotational character than ^{44}Ar.

The $E2$ matrix element linking the 2_2^+ and the 2_1^+ states is found to be large. The low level of statistics does not permit to extract the $M1$ matrix element for this transition. While the uncertainty due to a possible $M1$ contribution is included in the value for the $E2$ matrix element given in Table II, the uncertainty due to unknown couplings to higher-lying states is not included. A strong coupling of the 2_2^+ state to higher-lying states could reduce the $\langle 2_2^+ \| E2 \| 2_1^+ \rangle$ matrix element by up to 20%, even if the corresponding transitions are unobserved. Without further constraints on the feeding of the 2_2^+ state it was also impossible to determine its diagonal matrix element.

IV. COMPARISON WITH THEORY AND DISCUSSION

The present results represent the first direct measurement of the nuclear shape for an excited state in this neutron-rich region of the nuclear chart, and for the first time it was possible to extract matrix elements beyond the first 2^+ state in this region. In the following the experimental results are compared to calculations using different theoretical approaches and discussed in the wider context of the development of deformation in nuclei with $N \approx 28$ below ^{48}Ca. Experimental and theoretical values for excitation energies, $B(E2)$ values, and quadrupole moments for several nuclei in the region are summarized in Table III and presented in Fig. 3.

A. Shell model calculations

The new experimental results for ^{44}Ar, only two protons and two neutrons away from doubly magic ^{48}Ca, call for a comparison with shell model calculations. Extensive calculations have been performed by Retamosa *et al.* for the neutron-rich nuclei in the region of interest using the full *sd* and *pf* shells for protons and neutrons, respectively [8]. A new

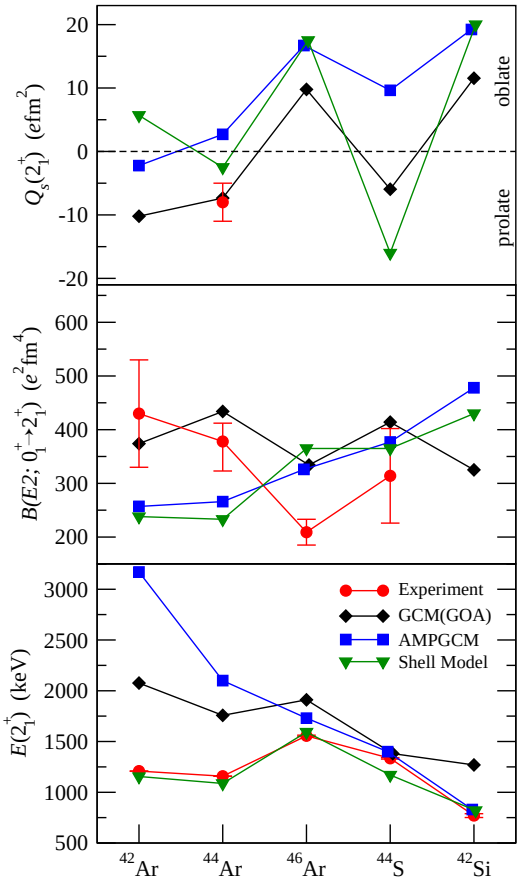


FIG. 3: (Color online) Graphical representation of the experimental and theoretical values from Table III showing the excitation energy of the 2_1^+ state (bottom), the $B(E2; 0_1^+ \rightarrow 2_1^+)$ value (center), and the spectroscopic quadrupole moment of the 2_1^+ state (top) for the neutron-rich argon isotopes $^{42-46}$Ar and along the chain of $N = 28$ isotones from ^{46}Ar to ^{42}Si.

effective interaction was derived in this work, and its parameters were fitted to known experimental data in the region. The results were in good agreement with the experimental excitation energies of the 2_1^+ states in the Ar isotopes [8]. However, large discrepancies appeared for the proton-deficient $N = 28$ isotones, in particular for ^{42}Si. Retamosa *et al.* had predicted that the $N = 28$ shell closure persists in the proton-deficient isotones and that ^{42}Si is a doubly-magic nucleus [8]. The same conclusion was also supported by shell model calculations using a truncated valence space [7].

As more experimental data became available in this mass region, the monopole component of the SDPF interaction was modified [36], and new calculations were performed for the $N = 28$ isotones [37]. With the modified interaction, SDPF-NR, the shell model calculations

TABLE III: Excitation energies (MeV), spectroscopic quadrupole moments ($e$fm^2), and $B(E2;0_1^+ \rightarrow 2_1^+)$ values (e^2fm^4) for the 2_1^+ states in ^{42}Ar, ^{44}Ar, ^{46}Ar, ^{42}S, ^{44}S, and ^{42}Si. For ^{44}Ar also the results for the 2_2^+ state are given. The experimental values are compared to the five-dimensional GCM(GOA) calculations, angular momentum projected GCM calculations restricted to axial shapes (AMPGCM), and to shell model calculations. Results for which no reference is given were obtained in the present work.

		Experiment	GCM(GOA)	AMPGCM	Shell Model
^{42}Ar	$E(2_1^+)$	1.208(1) [41]	2.076	3.17	1.155
	$Q_s(2_1^+)$	—	−10.2	−2.2	+5.7
	$B(E2;0_1^+ \rightarrow 2_1^+)$	430(100) [41]	374	257	238
^{44}Ar	$E(2_1^+)$	1.158(1)	1.758	2.10	1.087
	$E(2_2^+)$	2.011(1)	3.460	4.19	1.776
	$Q_s(2_1^+)$	−8(3)	−7.3	+2.7	−2.5
	$Q_s(2_2^+)$	—	+5.3	−0.5	+4.3
	$B(E2;0_1^+ \rightarrow 2_1^+)$	378^{+34}_{-55}	434	266	233
	$B(E2;0_1^+ \rightarrow 2_2^+)$	23(2)	1.77	1.51	100
	$B(E2;2_1^+ \rightarrow 2_2^+)$	680^{+150}_{-90}	139	—	88
^{46}Ar	$E(2_1^+)$	1.555(9) [17]	1.911	1.73 [13]	1.593
	$Q_s(2_1^+)$	—	+9.8	+16.7 [13]	+17.5
	$B(E2;0_1^+ \rightarrow 2_1^+)$	209(24) [16, 17]	334	326 [13]	365
^{42}S	$E(2_1^+)$	0.904(5) [14]	1.16	1.54 [13]	0.998
	$Q_s(2_1^+)$	—	−15.7	−16.0 [13]	−17
	$B(E2;0_1^+ \rightarrow 2_1^+)$	397(63) [16]	427	459 [13]	374
^{44}S	$E(2_1^+)$	1.334(7) [3, 14, 42]	1.38	1.40 [13]	1.17
	$Q_s(2_1^+)$	—	−5.9	+9.6 [13]	−16
	$B(E2;0_1^+ \rightarrow 2_1^+)$	314(88) [3]	414	377 [13]	365
^{42}Si	$E(2_1^+)$	0.770(19) [6]	1.269	0.83 [13]	0.82 [9]
	$Q_s(2_1^+)$	—	+11.5	+19.2 [13]	+20 [9]
	$B(E2;0_1^+ \rightarrow 2_1^+)$	—	325	478 [13]	430 [9]

found an increase of the $2p-2h$ intruder configuration for the ground-state wave functions in the $N = 28$ isotones. The intruder configuration was predicted to become dominant in the ground state of ^{40}Mg. However, the calculations still found a rather high excitation energy of 1.49 MeV for the 2_1^+ state in ^{42}Si [37]. When the excitation energy of this state was experimentally established to be only 770 keV [6], the monopole interaction was again modified to reproduce this result [9]. Using this latest version of the interaction, SDPF-U, and effective charges $\epsilon_\pi = 1.35\ e$ and $\epsilon_\nu = 0.35\ e$, the spectroscopic properties of neutron-rich Ar and S isotopes were calculated with the code ANTOINE [38–40]. The results are included in Table III and Fig. 3.

With the new SDPF-U interaction the shell model calculations reproduce the energies of the 2_1^+ states very well throughout the region. The $B(E2; 0_1^+ \rightarrow 2_1^+)$ values predicted for ^{42}Ar and ^{44}Ar are too small, while the one for ^{46}Ar is too large. The shell model calculations predict an increase of the $B(E2)$ values from ^{44}Ar to ^{46}Ar in contrast to the sharp drop which is observed experimentally. This increase of the $B(E2)$ values in the calculations is coinciding with a shape change from a very small prolate deformation in ^{44}Ar to a relatively large oblate deformation in ^{46}Ar. The predicted spectroscopic quadrupole moment $Q_s(2_1^+)$ in ^{44}Ar is somewhat smaller than the experimental value, but has the correct sign. The shell model predicts alternating oblate (^{46}Ar, ^{42}Si) and prolate (^{44}S, ^{40}Mg) shapes for the 2_1^+ states in the $N = 28$ isotones with relatively large deformation.

The above discussion illustrates a limitation of shell model calculations for exotic nuclei: The matrix elements of the effective interaction have to be adjusted to experimental observables within the region of interest. If experimental data is scarce, extrapolations to exotic nuclei can lead to significant deviations, as could be seen in the case of ^{42}Si. A satisfactory description of the spectroscopic properties throughout the region of interest was only possible after experimental data became accessible. In calculations based on the mean field approach, on the other hand, the effective interaction is derived not locally, but globally. Such models have consequently a better chance to describe at least the global trends in the structure of exotic nuclei. Calculations based on the mean-field approach and shell model calculations therefore generally provide complementary nuclear structure information.

B. Relativistic mean-field calculations

The region of proton-deficient $N \approx 28$ nuclei has been studied by Werner *et al.* using Skyrme Hartree-Fock and relativistic mean-field (RMF) calculations [10, 11]. Albeit differing in some details, both approaches predicted the onset of deformation in this mass region. Another detailed analysis of shape effects in the framework of RMF theory has been presented by Lalazissis *et al.* [12]. In the latter work the authors calculated ground-state properties such as the quadrupole deformation, proton and neutron radii, and two-neutron separation energies using a unified relativistic Hartree-Bogoliubov (RH+B) description of mean-field and pairing correlations with the NL3 effective interaction for the RMF Lagrangian and the pairing term of the Gogny D1S interaction. It was found that the spherical $N = 28$ shell closure is strongly suppressed resulting in deformed ground states and shape coexistence. The ground-state deformation of the $N = 28$ isotones was predicted to alternate between oblate in ^{46}Ar and ^{42}Si and prolate in ^{44}S and ^{40}Mg, in agreement with the predictions of the shell model. The importance of the correct description of pairing correlations was investigated by comparing the fully self-consistent RH+B calculations with results from a simplified RMF approach with BCS pairing and constant pairing gap (RMF+BCS). The most pronounced difference between the two calculations was found for the ground-state deformation of ^{44}Ar, which was predicted to be oblate in the RH+B, but prolate in the RMF+BCS calculation [12]. The prolate experimental quadrupole moment for the 2_1^+ state in ^{44}Ar seems to support the RMF+BCS calculation. One should, however, be careful with such a general conclusion about the pairing treatment from this result. The potential energy for ^{44}Ar is rather soft with respect to deformation, and the ground-state shape cannot be easily inferred from the spectroscopic quadrupole moment of the 2_1^+ state.

The RMF calculations describe only ground-state properties, and no angular momentum or particle number projection was performed. In order to compare calculations with spectroscopic observables related to excited states, the wave functions have to be transformed into the laboratory frame of reference. The fact that both prolate and oblate shapes are found nearly degenerate in energy furthermore suggests that shape coexistence may occur. To account for configuration mixing, correlations beyond the mean-field description have to be considered. Another deficiency of the mean-field calculations mentioned above is the fact that they do not correct for the zero point rotational energy.

C. Angular-momentum projected generator coordinate method

The above limitations of the mean-field approach can be overcome by calculations using the angular momentum projected generator coordinate method (AMPGCM) with the axial quadrupole moment as generator coordinate [13, 43]. The starting point in this approach is a set of axially symmetric wave functions from Hartree-Fock-Bogoliubov (HFB) calculations using the Gogny D1S interaction [44, 45] with constraints on the quadrupole moment q_{20}. The superposition amplitudes of the constrained wave functions are found after projection onto angular momentum in a variational approach as the solutions of the Hill-Wheeler-Griffin equation [46, 47]. The basis states are restricted to reflection-symmetric states, limiting the configuration mixing calculations to positive-parity states with even spin. Different states of the same spin and parity correspond either to different quadrupole deformation or to quadrupole-vibrational states. The AMPGCM allows the direct computing of spectroscopic observables such as $B(E2)$ values and spectroscopic quadrupole moments. The only parameters entering in the calculations are those of the Gogny D1S interaction, which have been universally adjusted and are valid for the entire nuclear chart. Details of the method are discussed in Ref. [43] and results for the $N = 28$ isotones can be found in Ref. [13]. New AMPGCM calculations for ^{42}Ar and ^{44}Ar have been performed in the present work. The results are included in Table III and Fig. 3.

The AMPGCM calculations predict the coexistence of oblate and prolate shapes throughout the region of proton-deficient $N \approx 28$ nuclei. The excitation energies found in the AMPGCM calculations for the $N = 28$ isotones are in good agreement with the experimental values [13]. In particular the very low-lying 2^+_1 energy in ^{42}Si was correctly predicted. However, the energy spectra calculated for the lighter Ar isotopes are much too stretched, and the excitation energies calculated for the 2^+_1 states in ^{42}Ar and ^{44}Ar are found significantly too high. One could remark that a model which uses the quadrupole deformation to characterize the states is not well adapted to describe near-spherical nuclei with a soft potential. The $B(E2)$ values found in the AMPGCM calculations are similar to those found by the shell model. The $B(E2; 0^+_1 \rightarrow 2^+_1)$ values for ^{42}Ar and ^{44}Ar are smaller than the experimental values, while the one for ^{46}Ar is too large. The small $B(E2)$ values for ^{42}Ar and ^{44}Ar are due to a strong mixing of prolate and oblate components in the wave functions of the 2^+_1 states. The 2^+_1 state in ^{46}Ar, on the other hand, is found with a rather pure

oblate character [13]. The calculations reproduce the experimentally observed increase of the $B(E2)$ values from ^{46}Ar to ^{44}S, but the systematic trend along the chain of Ar isotopes is not correctly described.

The AMPGCM calculations predict oblate quadrupole moments for the 2_1^+ states in the $N = 28$ isotones (except for ^{40}Mg). Pronounced shape coexistence is found in ^{44}S with similar energies for oblate and prolate states, resulting in strong mixing and a smaller quadrupole moment for the 2_1^+ state [13]. Strong mixing is also found for the wave functions in ^{42}Ar and ^{44}Ar. However, the deformations are smaller and the spectroscopic quadrupole moments for the 2_1^+ states are consequently found close to zero, slightly prolate for ^{42}Ar and slightly oblate for ^{44}Ar, contrary to the sign of the experimental value.

When comparing the AMPGCM calculations with other predictions in Fig. 3, one is inclined to suspect that the model is biased towards oblate shapes. This might be related to the fact that the model is restricted to axial deformations and vibrations, whereas in reality the nucleus has other degrees of freedom. In particular in a nucleus with a soft potential like ^{44}Ar one might expect γ vibrations to be a low-lying mode of excitation. As the γ degree of freedom lies outside the model space, the AMPGCM calculations cannot account for such excitations and seem to be biased towards axially symmetric oblate shapes due to a lack of other available excitation modes. In order to draw such a conclusion, however, it would be necessary to measure more quadrupole moments in neighboring nuclei. It is interesting to note that a similar bias towards oblate shapes was also observed in another region of prolate-oblate shape coexistence: axial GCM calculations using the same technique with a Skyrme interaction found the ground states of the neutron-deficient krypton isotopes to be dominated by oblate shapes [48], contrary to experimental evidence [49]. Configuration mixing calculations which included the triaxial degree of freedom, on the other hand, were able to reproduce the correct ordering of prolate and oblate states in this region of shape coexistence [49, 50].

D. Triaxial configuration mixing calculations

To extend the GCM calculations from axial to triaxal shapes represents a considerable task, since rotations about the three Euler angles also have to be considered, resulting in a five-dimensional collective coordinate. A formally exact solution of the GCM problem

including the triaxial degree of freedom has only very recently been attempted for the light nucleus ^{24}Mg [51]. Equivalent calculations for heavier nuclei are at present prohibitively time consuming. The task can be simplified by introducing the so-called Gaussian overlap approximation (GOA), which assumes the overlap of the GCM basis states to be Gaussian. The starting point for such calculations is again a set of wave functions from HFB calculations with the Gogny D1S interaction, but this time constrained to both axial and triaxial quadrupole parameters (q_{20}, q_{22}). The superposition amplitude of the correlated states is then again found as the solution of the Hill-Wheeler-Griffin equation [46, 47]. However, the use of the GOA transforms this integro-differential equation into a Schrödinger-like equation with a collective Bohr-like Hamiltonian.

The moments of inertia are calculated self-consistently [52] at rotational frequency close to zero ($\hbar\omega = 2$ keV). The collective masses are first calculated in the cranking approximation [53, 54] and then renormalized to fulfill their relationships with the moments of inertia along symmetry axes [55]. As a result the well known deficiencies of collective masses calculated in the Inglis-Belyaev approximation are alleviated. The renormalized masses are higher than before, in keeping with expectations based on the Thouless-Valatin prescription [52]. The implementation of this renormalization in the present GCM(GOA) approach, which remains parameter free, decreases the excitation energy of 0_2^+ states throughout the chart of nuclei and significantly reduces $B(E2)$ values in particular for medium and light-mass nuclei, which are soft against β and γ deformation. The new prescription and its implication for collective properties at low spin and excitation energy will be described in detail in a separate publication [56]. The method and the procedure to calculate excitation energies, transition probabilities, and spectroscopic quadrupole moments can be found in Ref. [57].

New HFB-based configuration-mixing calculations using the GCM(GOA) approach with the finite-range, density-dependent Gogny D1S effective interaction have been performed for ^{44}Ar and several neighboring even-even nuclei. Similar calculations had already been performed for the chain of neutron-rich sulfur isotopes [14]. Potential energy surfaces from the calculations for the argon isotopes and $N = 28$ isotones are displayed in Fig. 4. The isotopes ^{42}Ar and ^{44}Ar are found to be relatively soft. A well-localized oblate minimum is developing in ^{46}Ar in addition to a spherical minimum. For ^{44}S coexistence of prolate and oblate shape is predicted with two distinct minima separated by a triaxial barrier. Finally, the prolate minimum vanishes again for ^{42}Si, which is predicted to be a well-deformed

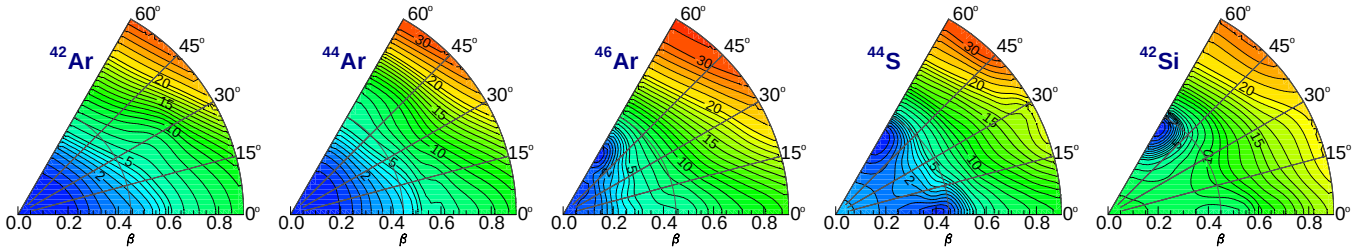


FIG. 4: (Color online) Potential energy surfaces over the (β, γ) plane from constrained HFB calculations with the Gogny D1S interaction and including a zero-point energy correction for (from left to right) ^{42}Ar, ^{44}Ar, ^{46}Ar, ^{44}S, and ^{42}Si.

oblate rotor. The calculated values for excitation energies, $B(E2)$ values, and spectroscopic quadrupole moments are included in Table III and Fig. 3.

The excitation energies of the 2_1^+ states found in the GCM(GOA) calculations are systematically too large for the nuclei in this region, with the exception of ^{44}S. Also the higher-lying states are generally predicted at too high excitation energies, as can be seen for the 2_2^+ state in ^{44}Ar. On the other hand, it seems that the triaxial calculations are less affected by the softness of the potential in ^{42}Ar and ^{44}Ar than the axial AMPGCM calculations. The systematic trend of the 2_1^+ energies is well reproduced, in particular the increase of $E(2_1^+)$ from ^{44}Ar to ^{46}Ar and the decrease along the chain of $N = 28$ isotones from ^{46}Ar to ^{42}Si. The calculations thus confirm the erosion of the shell closure, but it is obvious that the moments of inertia are not correctly described. The moments of inertia are calculated near rotational frequency zero, and the model assumes that they do not change with increasing frequency. This is usually a valid assumption for heavier well-deformed nuclei at low spin. For nuclei in the region of the present investigation, and in particular for the rather soft argon isotopes, this assumption is inappropriate, as was already concluded from the energy spectra of the $^{40-44}$S isotopes [14].

The new procedure to renormalize the collective masses has improved the agreement of the calculated $B(E2)$ values with experiment, despite the manifest discrepancies for the moments of inertia. The $B(E2; 0_1^+ \rightarrow 2_1^+)$ values for ^{42}Ar and ^{44}Ar, for example, have been reduced by approximately 30%. Although the absolute values are still slightly too large, the experimentally observed decrease from ^{44}Ar to ^{46}Ar and the increase from ^{46}Ar to ^{44}S are well reproduced. A difference between the axial and triaxial configuration mixing calculations

is observed not only for the Ar isotopes, but also for the $B(E2; 0_1^+ \rightarrow 2_1^+)$ value in ^{42}Si. Unfortunately, an experimental measurement of this value is presently out of reach.

The principal new result obtained from the experiment is the negative spectroscopic quadrupole moment for the 2_1^+ state in ^{44}Ar of $Q_s(2_1^+) = -8(3)$ $e$fm^2, indicating prolate shape. The GCM(GOA) calculation predicted $Q_s(2_1^+) = -7.3$ $e$fm^2 in agreement with the experimental value. Compared to the results of the axial GCM calculation, the quadrupole moments from the triaxial calculation are systematically shifted towards spherical and prolate shapes, resulting in alternating prolate and oblate shapes for ^{44}Ar, ^{46}Ar, ^{44}S, and ^{42}Si, respectively. Given the softness of the potential for some nuclei and the occurrence of prolate-oblate shape coexistence for others, such a shift seems at least plausible. With only one experimental data point, however, it is difficult to draw firm conclusions. The measurement of spectroscopic quadrupole moments in neighboring nuclei would shed more light on the validity of the different theoretical approaches.

The Coulomb excitation of ^{44}Ar resulted in the first experimental measurement of $B(E2)$ values beyond the 2_1^+ state in this region of the nuclear chart. A surprisingly large matrix element was found between the first and second 2^+ states, which seems difficult to explain. Due to the low level of statistics it was impossible to measure the quadrupole moment of the 2_2^+ state. The GCM(GOA) calculation finds significantly lower $B(E2; 2_1^+ \rightarrow 2_2^+)$ and $B(E2; 0_1^+ \rightarrow 2_2^+)$ values. The calculation predicts a positive spectroscopic quadrupole moment of $Q_s(2_2^+) = +5.3$ $e$fm^2. This value is consistent either with an oblate intrinsic shape and $K = 0$ or with a γ-vibrational $K = 2$ state based on a prolate intrinsic shape. The calculations clearly support the latter interpretation and find the $K = 2$ component in the wave function of the 2_2^+ state to be 80%. For the yrast sequence, on the other hand, the calculation finds an almost pure $K = 0$ character. The quadrupole moment is predicted to increase to -14 and -19 $e$fm^2 for the 4_1^+ and 6_1^+ states, respectively, showing the development of a sizable prolate deformation and rotational character with higher spin in the ground-state band. It is interesting to note that the axial AMPGCM calculations find a similar behavior with $Q_s(4_1^+) = -6.2$ $e$fm^2 and $Q_s(6_1^+) = -15.4$ $e$fm^2, pointing to a situation in which there is strong mixing of oblate and prolate configurations near the ground state, while prolate deformed states become dominant with increasing spin values along the yrast band.

The onset of deformation in the argon isotopes is also reflected in the recently measured

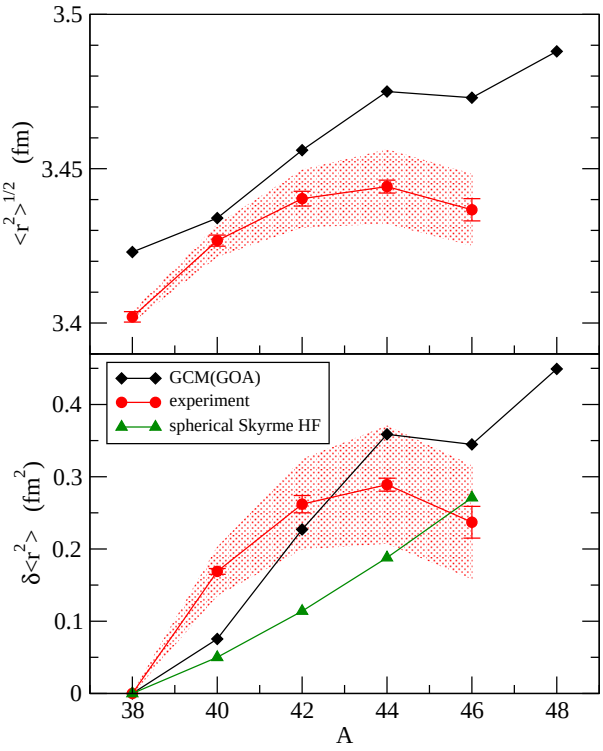


FIG. 5: (Color online) Mean-square charge radii (top) and isotope shifts relative to ^{38}Ar (bottom) for the even-mass Ar isotopes. The experimental values are taken from Blaum *et al.* [58] and compared to the GCM(GOA) and to spherical Skyrme SGII Hartree-Fock calculations [59]. The error bars on the experimental data represent the statistical errors only; systematic errors are indicated by the shaded areas.

mean-square charge radii obtained in collinear laser spectroscopy [58], which are shown in Fig. 5. The experimental radii show a parabolic trend superimposed on a monotonic increase, which was attributed to deformation effects. This behavior is consistent with the fact that spherical Skyrme Hartree-Fock calculations [59] only reproduce the monotonic increase with neutron number, but not the deformation-related decrease from ^{44}Ar to ^{46}Ar. The GCM(GOA) calculations, on the other hand, are in good agreement with the experimental data, both on an absolute scale and relative to ^{38}Ar. They reproduce in particular the decrease in radius from ^{44}Ar to ^{46}Ar.

Proton radii for the argon isotopes were also calculated by Lalazissis *et al.* [12]. Only the RMF calculation using BCS pairing reproduces the decrease in the charge radius from ^{44}Ar to ^{46}Ar, whereas the fully self-consistent RH+B calculation finds a smooth behavior without any pronounced shape effects. One should again be careful not to draw wrong conclusions

about the validity of the description of pairing from this result. Since the RMF+BCS model predicts a change from prolate ground state in ^{44}Ar to oblate in ^{46}Ar, it is only consistent that this shape transition is also reflected by the radii. Since the RH+B calculation predicts both ^{44}Ar and ^{46}Ar to be oblate, one would not expect a discontinuity in the radius between these two isotopes. The different behavior of the charge radii in the RMF+BCS and RH+B models is most likely related to the softness of the potential in ^{44}Ar than to the treatment of pairing.

V. SUMMARY AND CONCLUSIONS

The development of deformation in neutron-rich $N \approx 28$ nuclei was investigated in a low-energy Coulomb excitation experiment using a radioactive ^{44}Ar beam from the SPIRAL facility at GANIL. The Coulomb excitation cross section to the first and second 2^+ state was measured as a function of scattering angle and for two different target materials (^{109}Ag and ^{208}Pb). The three transitional $E2$ matrix elements connecting the 0_1^+, 2_1^+, and 2_2^+ states were extracted from the observed γ-ray yields together with the diagonal matrix element for the 2_1^+ state using the coupled-channel least-squares fitting code GOSIA. The $B(E2; 0_1^+ \rightarrow 2_1^+)$ value is in agreement with the value found in an intermediate-energy Coulomb excitation experiment. The shape connected to the 2_1^+ state is found to be prolate. These results represent the first direct measurement of a quadrupole moment and the first measurement of $B(E2)$ values beyond the 2_1^+ state in this region of neutron-rich nuclei.

The experimental results are compared to shell model and relativistic mean-field calculations, and to both axial and triaxial configuration-mixing calculations using the generator coordinate method with the Gogny D1S interaction. Using the latest effective interaction for calculations in the $sd - pf$ valence space, SDPF-U, the shell model is in very good agreement with the energies of the 2_1^+ states throughout the region, but cannot reproduce the systematic trend of $B(E2)$ values for the chain of Ar isotopes. Relativistic mean-field calculations describe the collapse of the $N = 28$ shell closure, but produce ambiguous results concerning the shape and charge radius of ^{44}Ar. Configuration mixing calculations including correlations beyond the mean field allow a direct comparison with spectroscopic observables. The angular-momentum projected generator coordinate method with the axial quadrupole deformation as generator coordinate and the Gogny D1S interaction describes

the properties of the $N = 28$ isotones well, but finds too large excitation energies and too small $B(E2)$ values for the soft nuclei ^{42}Ar and ^{44}Ar. Without taking into account the triaxial degree of freedom, the AMPGCM calculations seem to be biased towards oblate shapes. Five-dimensional configuration-mixing calculations using the GCM approach with Gaussian overlap approximation and the Gogny D1S interaction are in better agreement with the experimental excitation energies, but the spectra are still too dilated for the Ar isotopes. The systematic trends of the $B(E2)$ values are reproduced both for the Ar isotopes and for the $N = 28$ isotones, and the calculations are also able to reproduce the measured quadrupole moment in ^{44}Ar. They suggest furthermore a γ-vibrational character of the 2_2^+ state in ^{44}Ar. More experimental data on transition strengths and quadrupole moments in neighboring nuclei are clearly needed in order to draw further conclusions. Their measurement remains a challenging goal for future experiments.

Acknowledgments

This work was partly supported by the European Commission FP6 - Structuring the ERA - Integrated Infrastructure Initiative - Contract EURONS No. RII3-CT-2004-506065. The authors would like to thank the technical staff at GANIL for excellent support during the experiment and L. Gaudefroy and F. Nowacki for valuable discussions concerning shell model results.

---

[1] D. Guillemaud-Mueller, C. Detraz, M. Langevin, F. Naulin, M. de Saint-Simon, C. Thibault, F. Touchard, M. Epherre, Nucl. Phys. A **426**, 37 (1984).

[2] L. Gaudefroy *et al.*, Phys. Rev. Lett. **97**, 092501 (2006); A. Signoracci, B.A. Brown, Phys. Rev. Lett. **99**, 099201 (2007); L. Gaudefroy *et al.*, Phys. Rev. Lett. **99**, 099202 (2007).

[3] T. Glasmacher *et al.*, Phys. Lett. B **359**, 163 (1997).

[4] S. Grévy *et al.*, Eur. Phys. J. A **25**, s1, 111 (2005).

[5] L. Gaudefroy *et al.*, Phys. Rev. Lett., in press.

[6] B. Bastin *et al.*, Phys. Rev. Lett. **99**, 022503 (2007).

[7] J. Fridmann *et al.*, Nature(London) **435**, 922 (2005).

[8] J. Retamosa, E. Caurier, F. Nowacki, A. Poves, Phys. Rev. C **55**, 1266 (1997).

[9] F. Nowacki and A. Poves, Phys. Rev. C **79**, 014310 (2009).

[10] T.R. Werner, J.A. Sheikh, W. Nazarewicz, M.R. Strayer, A.S. Umar, M. Misu, Phys. Lett. B **335**, 259 (1994).

[11] T.R. Werner, J.A. Sheikh, M. Misu, W. Nazarewicz, J. Rikovska, K. Heeger, A.S. Umar, M.R. Strayer, Nucl. Phys. A **597**, 327 (1996).

[12] G.A. Lalazissis, D. Vretenar, P. Ring, M. Stoitsov, L.M. Robledo, Phys. Rev. C **60**, 014310 (1999).

[13] R. Rodríguez-Guzmán, J.L. Egido, L.M. Robledo, Phys. Rev. C **65**, 024304 (2002).

[14] D. Sohler *et al.*, Phys. Rev. C **66** 054302 (2002).

[15] S. Péru, M. Girod, J.F. Berger, Eur. Phys. J. A **9**, 35 (2000).

[16] H. Scheit *et al.*, Phys. Rev. Lett. **77**, 3967 (1996).

[17] A. Gade *et al.*, Phys. Rev. C **68**, 014302 (2003).

[18] T. Baumann et al., Nature(London) **449**, 1022 (2007).

[19] B. Fornal *et al.*, Eur. Phys. J. A **7**, 147 (2000).

[20] J. Mrázek *et al.*, Nucl. Phys. A **734**, E65 (2004).

[21] S. Wan *et al.*, Eur. Phys. J. A **6**, 167 (1999).

[22] H. Scheit *et al.*, Phys. Rev. C **63**, 014604 (2000).

[23] C.A. Bertulani, A.E. Stuchbery, T.J. Mertzimekis, A.D. Davies, Phys. Rev. C **68**, 044609 (2003).

[24] W. Mittig, J. Phys. G: Nucl. Part. Phys. **24**, 1331 (1998).

[25] L. Maunoury *et al.*, in Proceedings of the 13th Int. Workshop on ECR Ion Sources, College Station, 1997, edited by D.P. May and J.E. Ramirez (unpublished).

[26] D. Cline, Ann. Rev. Nucl. Part. Sci. **36**, 683 (1986).

[27] J. Simpson *et al.*, Acta Phys. Hung. N.S. **11**, 159 (2000).

[28] R.L. Robinson, F.K. McGowan, P.H. Stelson, W.T. Milner, Nucl. Phys. A **150**, 225 (1970).

[29] J. Blachot, Nucl. Data Sheets **107**, 355 (2006).

[30] T. Czosnyka, D. Cline, C.Y. Wu, Bull. Amer. Phys. Soc. **28**, 745 (1983).

[31] K. Alder and A. Winther, *Electromagnetic Excitation* (North-Holland, Amsterdam, 1975).

[32] F. Bosch and H. Spehl, Z. Phys. A **280**, 329 (1977).

[33] R. Brenn, H. Spehl, A. Weckherlin, H.A. Doubt, G. van Middelkoop, Z. Phys. A **281**, 219

(1977).

[34] J.A. Cameron and B. Singh, Nucl. Data Sheets **88**, 299 (1999).

[35] K. Nakai, F.S. Stephens, R.M. Diamond, Phys. Lett. B **34**, 389, (1971).

[36] S. Nummela *et al.*, Phys. Rev. C **63**, 044316 (2001).

[37] E. Caurier, F. Nowacki, A. Poves, Nucl. Phys. A **742**, 14 (2004).

[38] E. Caurier, ANTOINE code, IReS, Strasbourg 1989-2004.

[39] E. Caurier, F. Nowacki, Acta Phys. Pol. B **30**, 705 (1999).

[40] E. Caurier, G. Martinez-Pinedo, F. Nowacki, A. Poves, A.P. Zucker, Rev. Mod. Phys. **77**, 427 (2005).

[41] T.R. Fisher, T.T. Bardin, J.A. Becker, B.A. Watson, Phys. Rev. C **9**, 598 (1974).

[42] J. Fridmann *et al.*, Phys. Rev. C **74**, 034313 (2006).

[43] R. Rodríguez-Guzmán, J.L. Egido, R.M. Robledo, Nucl. Phys. A 709, 201 (2002).

[44] J. Dechargé, D. Gogny, Phys. Rev. C **21**, 1568 (1980).

[45] J.-F. Berger, M. Girod, and D. Gogny, Comput. Phys. Commun. **63**, 365 (1991).

[46] D.L. Hill and J.A. Wheeler, Phys. Rev. **89**, 1102 (1953).

[47] J.J. Griffin and J.A. Wheeler, Phys. Rev. **108**, 311 (1957).

[48] M. Bender, P. Bonche, P.-H. Heenen, Phys. Rec. C **74**, 024312 (2006).

[49] E. Clément *et al.*, Phys. Rev. C **75**, 054313 (2007).

[50] M. Girod, J.-P. Delaroche, A. Görgen, A. Obertelli, submitted to Phys. Lett. B.

[51] M. Bender and P.-H. Heenen, Phys. Rec. C **78**, 024309 (2008).

[52] D.J. Thouless and J.G. Valatin, Nucl. Phys. A **31**, 211 (1962).

[53] D.R. Inglis, Phys. Rev. **103**, 1786 (1956).

[54] S.T. Belyaev, Nucl. Phys. A **24**, 322 (1961).

[55] K. Kumar and M. Baranger, Nucl. Phys. A **92**, 608 (1967).

[56] J. Libert *et al.*, to be published.

[57] J. Libert, M. Girod, J.-P. Delaroche, Phys. Rev. C **60**, 054301 (1999).

[58] K. Blaum, W. Geithner, J. Lassen, P. Lievens, K. Marinova, R. Neugart, Nucl. Phys. A **799**, 30 (2008).

[59] A. Klein *et al.*, Nucl. Phys. A **607**, 1 (1996).